Kinematics, singularity, and workspace analysis of a spatial parallel robot with pure translational motion in a plane for pick-and-place operations

Adriyan[1*], Muhammad Ridha Fauzi[2], Zaki Anwar[1], Dimas Ahmad Mutaqin[1]

[1]Department of Mechanical Engineering, Universitas Muhammadiyah Riau, Pekanbaru, 28292, Indonesia
[2]Department of Vocational Automotive Engineering, Universitas Muhammadiyah Riau, Pekanbaru, 28292, Indonesia
*Corresponding author: adriyan@umri.ac.id

Abstract

This research presents a new spatial Parallel Manipulator (PM) with pure translational motion in a plane or 2-DOF PM for pick-and-place operation. This spatial 2-DOF PM is constructed by the 2($\underline{R}$RR)-2(PRRR) kinematic chain and is named Ψ2. This Ψ2 PM offers simplicity in its architecture because each limb applies a 1-DOF joint. The applicability of Ψ2 for pick-and-place operations was investigated by performing kinematic and singularity analyses at the preliminary stage. The singularity of Ψ2 was determined by relying on its Jacobian matrices, where three kinds of singularity can be evaluated. Next, the singularity and Jacobian matrix hold a key to identifying the workspace in a regular geometrical shape required for the operation of such an application. The identified operational workspace must be free of singularity and good conditioning workspace. In this study, two predetermined values of Ψ2 kinematic parameters were used to evaluate the kinematic characteristics and singularity of the manipulator as well as to identify its operational workspace. According to the results, Ψ2 has a good prospect of being applied to high-speed pick-and-place operations.

Keywords:
2-DOF parallel manipulator, pick-and-place operation, conditioning index, identified operational workspace.

1 Introduction

Pick-and-place operation is a common means for handling goods in the electronic, pharmacy, and food processing industries [1]. This operation involves translational motion in three-dimensional space (3T) and one rotational motion about a particular axis (1R), also known as a Schönflies motion. This motion can be achieved using serial manipulators, such as SCARA [2], or parallel manipulators [3]. Parallel Manipulators (PMs) provide more advantages over their serial counterparts in terms of speed, acceleration, stiffness, weight, payload-to-weight ratio, and dynamic characteristics [4]. Several parallel architectures, including Par4 [5], Pantopteron-4 [6], X4 [7], TH-SR4 [8], and TH-HR4 [3], have been developed for PMs with Schönflies motion.

In certain applications, pick-and-place operations can be performed without relying on the Schönflies motion itself. Additionally, the pick-and-place operation can be carried out using pure translational motion in space (3T) or even pure translational motion in the plane (2T). The latter option (2T) allows a simpler architecture and less complex control scheme

than 3T or 3T1R [9]. Pure translational motion (2T), also known as a two-degree of freedom (2-DOF) PM, is applied to a 5R Planar Parallel Manipulator (PPM) [10] and its variant. The workspace can be oriented either horizontally or vertically. The horizontal version can be considered the parallel version of SCARA and is achieved by replacing parts of its first two serial chains, as implemented in DexTAR [11] and 2($\underline{R}$RR)-RP [12]. In this context, R denotes the revolute joint, P represents the prismatic joint, and the underscore sign indicates the actuated joint.

On the other hand, the vertical version of the 2-DOF PM can be applied directly to pick-and-place operations using either planar or spatial architectures. The Diamond PM, a modified 5R PPM with a parallelogram chain (Pa) at one or both limbs, is an example of a planar architecture [9]. This manipulator has been successfully applied in production lines for quality inspection of rechargeable batteries. Thus, Meng *et*. *al*. [13] proposed V2, utilizing the PaUU-PaRR kinematic chain for the planar architecture of pick-and-place operation. This manipulator has an innovative design configuration that uses parallelogram chains and universal joints (U), providing high translational capability for high-speed operation.

The spatial structure is designed to alleviate the out-of-plane stiffness, which is the main drawback for planar structures, as demonstrated by Par2 [14], [15] and IRSBot-2 [16], [17]. Nurahmi [18] described 27 different 2-DOF PM architectures based on planar and spatial architectures, including previously proposed designs. These architectures were synthesized using the screw theory, resulting in 2-DOF PMs with 2, 3, and 4 limbs. Thus, these 27 architectures were optimized for two objective functions: the complexity of the kinematic chain (minimization) and the stiffness (maximization). As a result, eight out of 27 architectures were found to be the optimal architectures after the application of the Pareto front.

Furthermore, these eight architectures are the best candidates for pick-and-place operations using 2-DOF PMs; please refer to Figure VI.2 and Table VI.1 in [18]. However, there is one architecture that can be categorized as the best compromise between complexity and stiffness among these eight architectures. This best compromise value is the architecture constructed by a 2($\underline{R}$RR)-2(PRRR) kinematic chain. Therefore, this study proposes a new 2 DoF parallel manipulator named by Ψ2 using this 2($\underline{R}$RR)-2(PRRR) kinematic chain.

Ψ2 has the main features: (1) less complexity with high stiffness, (2) can keep its moving platform to stay parallel to the flat ground during its motion thanks to its passive limbs. A comprehensive investigation is required to realize Ψ2 for the real-world applications, especially for high-speed pick-and-place operations. Hence, this study was conducted to analyze the kinematics, singularity, and workspace of Ψ2 for achieving such an application. This analysis gives an insightful identification of its operational workspace using its kinematic performance index. The remainder of this manuscript is organized as follows: (1) section 2 comprises the sequence of steps taken to perform this research, (2) the findings during the investigation are presented and discussed in section 3, and (3) section 4.

2 Research Methods/Materials and Methods

This study presents the kinematic and singularity analysis of Ψ2, a new spatial PM with pure translational motion in the plane using the 2($\underline{R}$RR)-2(PRRR) kinematic chain. This analysis is initiated by applying the joint-and-loop graph and the kinematic diagram to represent its structure, as shown in Fig. 1(a). All the joint axes in each limb are arranged in parallel. The first two joints of the PR on the PRRR limb can also be replaced with a cylindrical (C) joint. Hence, Ψ2 can have another equivalent kinematic chain, 2($\underline{R}$RR)-2(CRR), whose joint-and-loop graph is shown in Fig. 1(b). Moreover, the kinematic diagram of Ψ2 and its equivalent is depicted in Fig. 2.
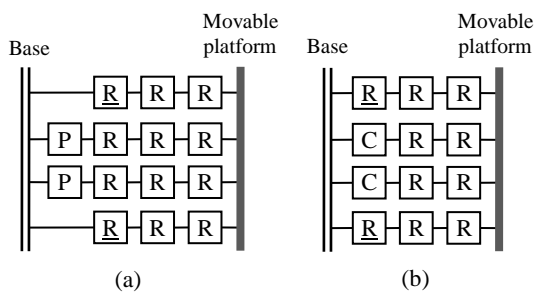
Fig. 1. Joint-and-loop graph for the (a) 2(R̲RR)-2(PRRR) and (b) 2(R̲RR)-2(CRR) kinematic chains.

In general, Ψ2 and its equivalent kinematic chain consist of a base, a movable platform, and four limbs. For construction, the base is connected to the movable platform by utilizing these four limbs arranged axisymmetric about the Z-axis. The RRR limbs are indicated by limb 1 and 2 and are situated on the XZ-plane, as displayed in Fig. 2. Moreover, the PRRR limbs (limb 3 and 4) lie on the perpendicular plane to the active limbs, i.e., the YZ-plane.
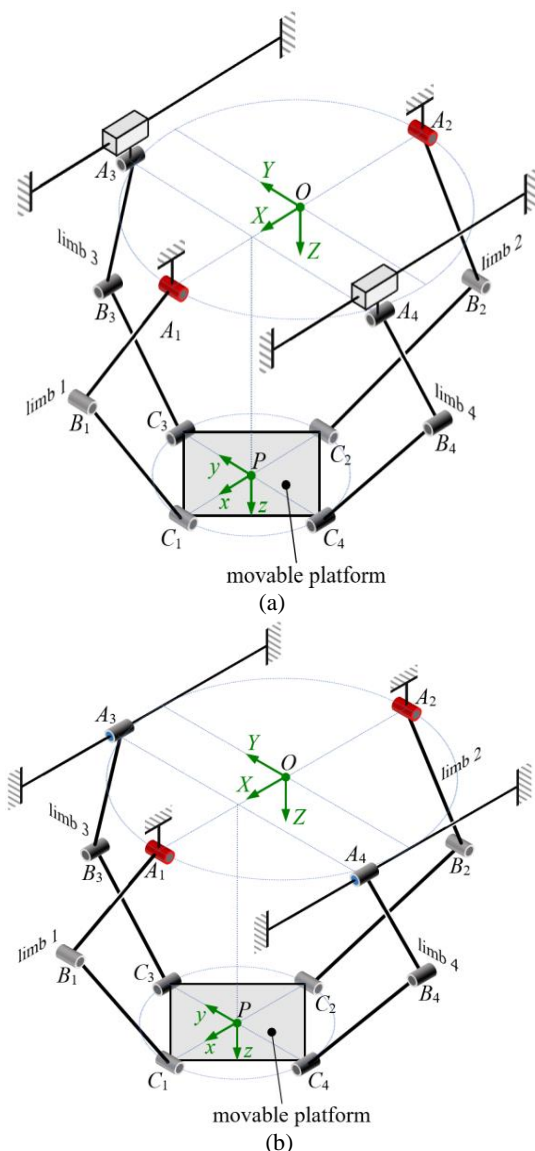

Fig. 2. Kinematic diagram of the (a) 2(R̲RR)-2(PRRR) and (b) 2(R̲RR)-2(CRR) kinematic chains, where the actuated revolute joints are colored red, as indicated in A_1 and A_2.

Then, a description of Ψ2 in terms of its configuration and mobility can be introduced. However, the manipulator was synthesized as a spatial PM with pure translational motion in the plane (2-DOF). The mobility of Ψ2 is still described briefly by applying the Grübler-Kutzbach (GK) formula and a screw theory based on observation methods.

The position equation can be formulated by referring to its kinematic diagram. This equation governs the displacement relationship between each kinematic chain and the platform. This position equation can be solved to obtain the solutions for its inverse and direct kinematic problem. The inverse and direct kinematic solutions are calculated to obtain their closed-form and numerical solutions. Moreover, this numerical solution is obtained by employing interval analysis because it has been applied in diverse areas, especially in robotics [19], [20]. Interval analysis can produce all real solutions in the nonlinear algebraic equations that govern the position equation. An interested reader should refer to the references [21] to gain more insight into this subject. The calculations for the inverse and direct kinematic solutions in closed-form and numeric form are utilized to check the solutions when using predetermined values for kinematic parameters.

The velocity equation can be obtained by taking the derivative of the position equation with respect to time once. Then, the velocity equation is rewritten in compact form to generate the Jacobian of the inverse and direct kinematics. These Jacobians can be used to analyze the singularity of Ψ2 by examining whether these matrices are rank deficient. Three kinds of singularities based on the Jacobians are evaluated to determine under which conditions the Ψ2 performance degenerates.

Furthermore, the Jacobian matrix is utilized to determine the conditioning index of Ψ2. In this study, the conditioning index is applied as a main performance index to identify a workspace that is useful for pick-and-place operation. This identified workspace is referred to as the operational workspace and is commonly defined as a simple 2D or 3D geometrical object, such as a square, rectangle, cylinder, cube, or rectangular prism. This workspace is characterized by the largest shape in a rectangular (or a square) form inside a Good-Condition Workspace (GCW). The GCW is a workspace where the Local Conditioning Index (LCI) is greater than 0.5 [22]. This study utilizes NumPy [23] and JuliaInterval [24] for numerical and interval calculations, respectively.

3 Results and Discussion

3.1 Mobility of Ψ2

The mobility of Ψ2 can be determined by referring to Fig. 2. It shows the number of links and joints possessed by Ψ2 and its equivalent kinematic chain. Ψ2 possesses 12 links and 14 joints, while 2(R̲RR)-2(CRR) has 10 links and 12 joints. The application of the GK formula [22] for Ψ2 and its equivalent kinematic chain results in a mobility of -4, which means that the manipulators are classified as over constrained manipulators. The mobility of an over-constraint PM can be determined using the modified GK formula, which essentially integrates the screw theory, as presented by [25]. From an architectural point of view, Ψ2 is similar to Par2 [15] which has active and passive limbs. In contrast, Ψ2 has less complexity compared to Par2 which uses 2(R(Pa_S))-2(R̲(Pa_S)), in terms of the number of links and joints used, according to its complexity index [26] and referring to work [18]. Here, Pa_S is a spatial parallelogram chain with Spherical (S) joints.

Furthermore, the screw theory can be applied to determine mobility by simply observing the motion and constraining forces and moments at each limb and the movable platform. The direction of all the joint axes present in Ψ2 and its equivalent kinematic chain is required for the first setup. All the joint axes in each limb of both kinematic chains are perpendicular to each respective plane. In this case, all joint axes of the active limbs and the passive limbs have a direction to the +Y-axis and +X-axis, respectively. Each limb that consists of an RRR kinematic chain produces a general planar motion, i.e. 2T and 1R at its respective plane. Thus, the presence of the P-joint at the PRRR limbs enables that limb to gain another motion in the X-direction. Hence, each RRR limb generates general planar motion in the XZ-plane. Moreover, each PRRR limb can undergo general planar motion in

the *YZ*-plane and translational motion perpendicular to this *YZ*-plane.

The constraint forces or moments that constrain those limbs can be determined as reciprocal conditions to the motion generated by each respective limb. The RRR limbs are constrained by one force in the *Y*-axis and two moments about the *X*- and *Z*-axes. Then, the PRRR limbs are constrained by two moments about the *Y*- and *Z*-axes. Furthermore, all the limbs connecting the base and movable platform constrain the platform as a result of the combination of constraints on each limb. These constraints on the platform include one constrained force on the *Y*-axis and three constrained moments about the *X*-, *Y*-, and *Z*-axes. Consequently, these constraints establish translational motion on the platform in the *X*- and *Z*-axes. Hence, Ψ2 and its equivalent kinematic chain have a mobility of 2-DOF in the *XZ*-plane.

The limb with the RRR chain is an active limb because its first joint (R) is actuated, while the PRRR chain is a passive limb. Each limb, whether active or passive, consists of a distal and proximal link. The distal link connects two revolute joints, A_i and B_i, where i denotes the limb number. Then, the proximal link connects the two revolute joints B_i and C_i. The lengths of the distal and proximal links are denoted by a and b, respectively, and are the same for each active and passive limb. Moreover, the distance between point A_1 and point A_2 through point O in the middle is equal to two times of the base radius r_B. Additionally, the distance between points A_3 and A_4 is equal to the length of A_1A_2. Finally, the position of point C_i toward point P is equal to the radius of the movable platform r_P.

Four parameters characterize Ψ2, denoted by r_B, a, b, and r_P; these parameters are known as kinematic parameters. To produce numerical results, these kinematic parameters must be defined with numerical values. At this stage, we selected numerical values for two sets of kinematic parameters, which are given in Table 1. For Ψ2, we will only consider the positive part of its workspace along the *Z*-direction.

Table 1. Two sets of numerical values for the kinematic parameters of the manipulator are shown in Fig. 2, where the dimensions are defined in mm.

Case	r_B	a	b	r_P
#1	100	270	400	30
#2	100	335	335	30

3.2 Position Analysis

The previous section extensively addressed the architecture of the manipulator. The position equation can be determined by referring to Fig. 3 for the view of the *XZ*-plane. Then, for the active limb itself, the position of point P can be defined by using the loop-closure equation (Eq. 1)

$$\mathbf{p} = \mathbf{r}_i + \mathbf{a}_i + \mathbf{b}_i + \mathbf{c}_i, \qquad (1)$$

for $i = 1, 2$. The vectors given in Eq. 1 are $\mathbf{p} = (x \ z)^T$, $\mathbf{r}_1 = (r_B \ 0)^T$, $\mathbf{r}_2 = (-r_B \ 0)^T$, $\mathbf{a}_i = a(\sin\theta_i \ \cos\theta_i)^T$, $\mathbf{b}_i = b(\sin\beta_i \ \cos\beta_i)^T$, $\mathbf{c}_1 = (-r_P \ 0)^T$, and $\mathbf{c}_2 = (r_P \ 0)^T$.

In this manipulator, the joints at A_1 and A_2 are the active joints, while the joints at B_1 and B_2 are the passive joints. The passive joint angles can be eliminated by arranging Eq. 1 and applying the dot product for each side. This yields Eq. 2

$$(\mathbf{p} - \mathbf{r}_i - \mathbf{a}_i - \mathbf{c}_i) \cdot (\mathbf{p} - \mathbf{r}_i - \mathbf{a}_i - \mathbf{c}_i) = \mathbf{b}_i \cdot \mathbf{b}_i, \qquad (2)$$

or it can be rewritten as Eq. 3

$$x_i^2 - 2ax_i\sin\theta_i + z^2 - 2az\cos\theta_i + a^2 - b^2 = 0, \qquad (3)$$

where $x_1 = x - r_B + r_P$, and $x_2 = x + r_B - r_P$. The term $r_B - r_P$ can be unified as a kinematic parameter r.
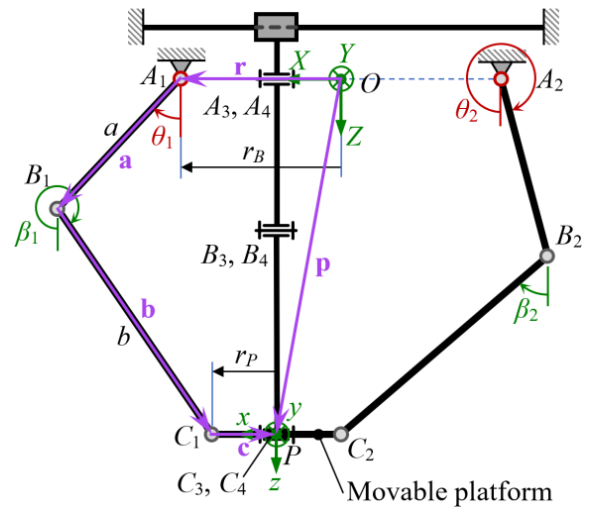

Fig. 3. View of the manipulator on the *XZ*-plane.

3.2.1 The Inverse Kinematic Problem

Afterward, the solution for the Inverse Kinematic Problem (IKP) can be determined to obtain the values of the actuated joints, θ_1, and θ_2, as the actuator space for the given position of points P, x, and z. It is expressed mathematically as Eq. 4.

$$\theta_i = 2\tan^{-1}\left(\frac{x_i + \lambda\sqrt{x_i^2 + z^2 - K_i^2}}{z + K_i}\right), \qquad (4)$$

where

$$K_i = \frac{x_i^2 + z^2 + a^2 - b^2}{2a}, \qquad (5)$$

for $i = 1, 2$; and λ is the branch index which has values of +1 and -1. The sign of this branch index indicates that the manipulator has four kinds of assembly modes: (+, +); (+, -); (-, +); and (-, -). An arrangement of this manipulator in Fig. 3 shows that it has the (+, -) assembly mode.

The closed-form solution in Eq. 4 is evaluated using the kinematic parameters in Table 1 (Case #1) for the position of point P, which is (200, 500) mm. Then, the roots of Eq. 3 can be computed to obtain the interval solution for the given position. Table 2 compares the evaluated closed-form solution and the interval solution. The subscripts + and – at θ_i denote the positive and negative signs of the branch index, respectively.

The application of interval analysis successfully determines the inverse kinematic solution of Ψ2. It provides both lower and upper bounds for the solutions. Each interval solution is bracketed by the respective closed-form solution. Thus, the pairs of closed-form solutions that constitute the assembly modes can be visualized to represent their physical appearance, as shown in Fig. 4.

Table 2. The evaluated closed-form and interval solutions for the IKP when P is at (200, 500) mm. All angular solutions are defined in rad.

θ_i	Closed-form solution	Interval solution
θ_{1+}	0.98023298	[0.980232, 0.980233]
θ_{1-}	-0.86037667	[-0.860377, -0.860376]
θ_{2+}	1.16087314	[1.160870, 1.160880]
θ_{2-}	-0.50539612	[-0.505397, -0.505396]

3.2.2 The Direct Kinematic Problem

On the other hand, the solution of the Direct Kinematic Problem (DKP) can be found by solving Eq. 3 for the positions of points P, x, and z, when the actuator spaces, θ_1 and θ_2, are known. Solving for z can be performed by treating z as a constant that reduces Eq. 3 into a second-order polynomial in x,

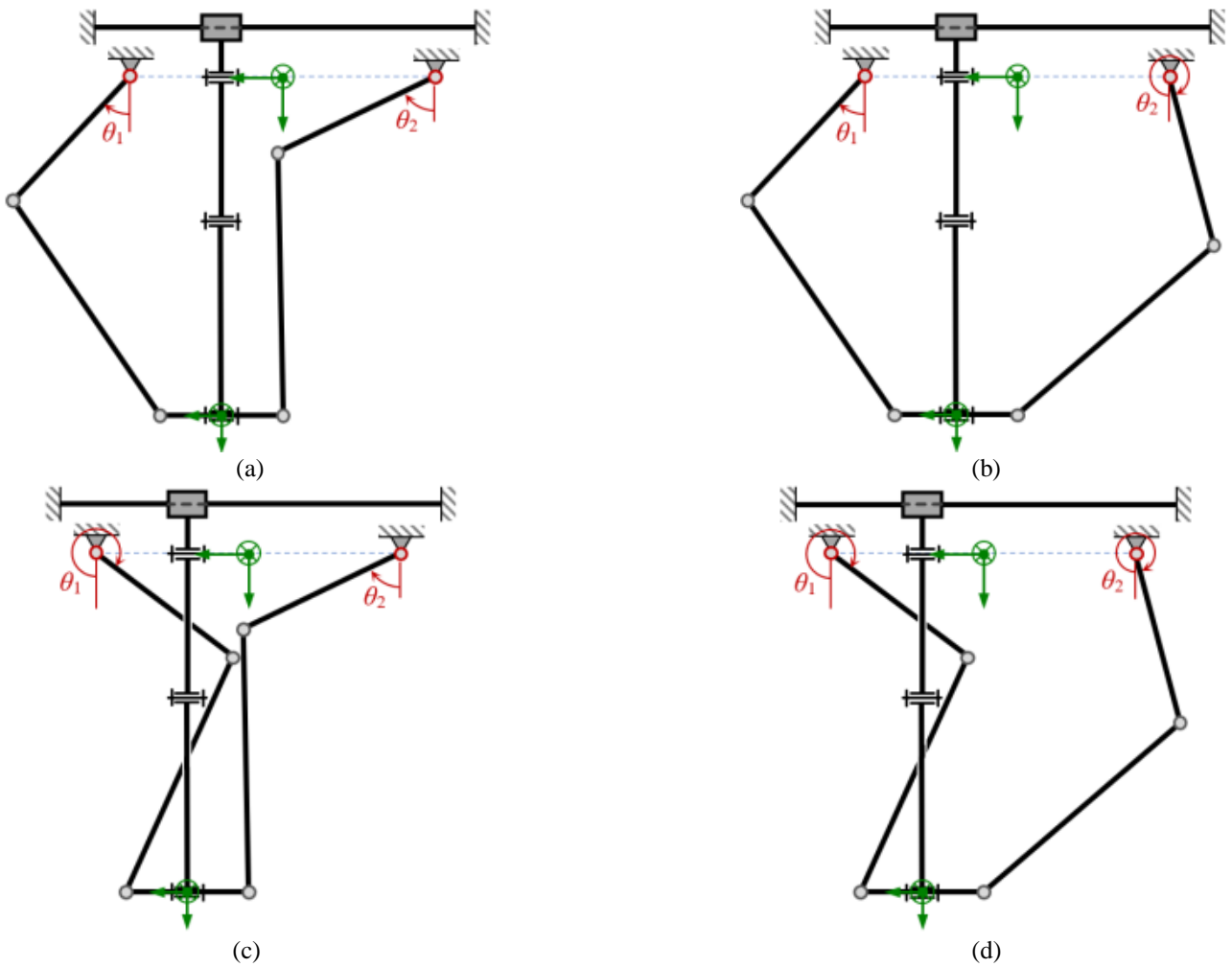$$x^2 - 2G_{xi}x + G_{xi}^2 + (z - G_{zi})^2 - b^2 = 0, \qquad (6)$$

Fig. 4. The assembly modes for the inverse kinematic solutions: (a) (+, +), (b) (+, -), (c) (-, +), and (d) (-, -).

for $i = 1, 2$, where $G_{x1} = r_B - r_P + a \sin\theta_1$, $G_{x2} = -r_B + r_P + a \sin\theta_2$, and $G_{zi} = a \cos\theta_i$.

Afterward, Sylvester's dialytic elimination method can be applied to Eq. 6, which results in a second-order polynomial in z. This process is given by Eq. 7.

$$4H_2 z^2 - 4H_1 z + H_0 = 0. \tag{7}$$

Hence, the solution for z can be obtained as the root of this second-order polynomial by relation Eq. 8

$$z = \frac{H_1 \pm \sqrt{H_1^2 - H_0 H_2}}{2H_2}, \tag{8}$$

where $H_2 = (G_{x1} - G_{x2})^2 + (G_{z1} - G_{z2})^2$, $H_1 = H_2 (G_{z1} + G_{z2})$, and $H_0 = (H_2 - 4b^2)(G_{x1} - G_{x2})^2 + H_2 (G_{z1} + G_{z2})^2$.

Once the solution for z is obtained, it can be used to determine the solution for x using Eq. 6 by subtracting the equation for $i = 1$ from the equation for $i = 2$. Thus, we have Eq. 9

$$x = \frac{G^2 - 2(G_{z1} - G_{z2})z}{2(G_{x1} - G_{x2})}, \tag{9}$$

where $G^2 = G_{x1}^2 - G_{x2}^2 + G_{z1}^2 - G_{z2}^2$.

Eq. 8 and Eq. 9 indicate that the manipulator has a closed-form solution for the DKP. The direct kinematic solution in Eq. 8 and Eq. 9 leads to two solutions. These solutions are two pairs of (x_+, z_+) and (x_-, z_-), where subscript + and − denote the positive and negative signs of the value under the roots in Eq. 8, respectively. Analogous to the inverse kinematic solution, the closed-form solution is evaluated for given values of actuator space θ_1 and θ_2

of $(\pi/3, -\pi/8)$ rad, respectively. Case #1 is selected for evaluation of the direct kinematic solution in terms of its kinematic parameters. Again, the roots of Eq. 3 are determined for that value of the actuator space.

Consequently, the interval solution gives a guaranteed bound for the evaluated closed-form solution. The first pair of solutions (x_+, z_+) for the evaluated closed-form solution of (138.93703, 499.43291) mm is bounded by the interval box of [138.9370, 138.9371] mm × [499.4329, 499.4330] mm. Moreover, the second pair of solutions (x_-, z_-) for the evaluated closed-form solution is (-8.434701, -114.985436) mm and lies within the interval box of [-8.4347012, -8.4347011] mm × [-114.98544, -114.98543] mm. Finally, the direct kinematic solution of Ψ2 can be presented in its physical representation, as shown in Fig. 5.

The existence of a closed-form solution for the DKP allows an efficient implementation for real-time position control and gravity compensation, as reported by [27]. It means that Ψ2 can benefit from this closed-form solution of its DKP when applying a real-time position control in the future.

3.3 Velocity and Jacobian

The velocity equation of Ψ2 can be found by differentiating Eq. 3 to time once. It can be expressed mathematically as Eq. 10.

$$a(x_i \cos\theta_i - z \sin\theta_i)\dot{\theta}_i = (x_i - a\sin\theta_i)\dot{x} + (z - a\cos\theta_i)\dot{z} \tag{10}$$

for $i = 1, 2$. This equation can be further expanded and presented in compact form as Eq. 11

$$\mathbf{J}_q \dot{\mathbf{q}} = \mathbf{J}_x \dot{\mathbf{x}}, \tag{11}$$

where $\dot{\mathbf{q}} = (\dot{\theta}_1 \quad \dot{\theta}_2)^T$ and $\dot{\mathbf{x}} = (\dot{x} \quad \dot{z})^T$.
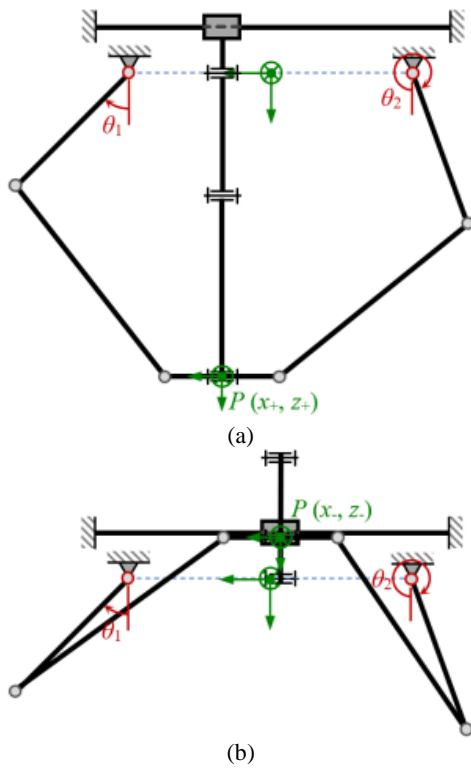
Fig. 5. Two configurations for the direct kinematic solutions based on the x and z pairs in Eq. 7 and Eq. 8: (a) (x_+, z_+) and (b) (x_-, z_-).

Here, $\mathbf{J}_q$ is the Jacobian of the inverse kinematic that forms a diagonal matrix where its element is filled by $a(x_i \cos\theta_i - z\sin\theta_i)$, for $i = 1, 2$, or

$$\mathbf{J}_q = a \begin{bmatrix} x_1\cos\theta_1 - z\sin\theta_1 & 0 \\ 0 & x_2\cos\theta_2 - z\sin\theta_2 \end{bmatrix}. \qquad (12)$$

Then, $\mathbf{J}_x$ is the Jacobian of the direct kinematic that is stated in matrix form as Eq. 13.

$$\mathbf{J}_x = \begin{bmatrix} x_1 - a\sin\theta_1 & z - a\cos\theta_1 \\ x_2 - a\sin\theta_2 & z - a\cos\theta_2 \end{bmatrix}. \qquad (13)$$

Furthermore, the Jacobian matrix can be determined by applying the relation [22] as Eq. 14.

$$\mathbf{J} = \mathbf{J}_q^{-1}\mathbf{J}_x. \qquad (14)$$

3.4 Singularity Analysis and Workspace

The singularity of the manipulator can be determined when the matrices $\mathbf{J}_q$ and $\mathbf{J}_x$ are rank deficient. Then, the first kind of singularity, or the inverse kinematic singularity, is given mathematically by $|\mathbf{J}_q| = 0$ [22], or

$$(x_1\cos\theta_1 - z\sin\theta_1)(x_2\cos\theta_2 - z\sin\theta_2) = 0. \qquad (15)$$

Eq. 15 provides a solution for both actuation angles, $\theta_1 = \tan^{-1}(x_1/z)$ and $\theta_2 = \tan^{-1}(x_2/z)$. This solution is fulfilled by a condition where the first and the second active limbs are fully extended or folded, as illustrated in Fig. 6. This singularity defines the boundary of the workspace for Ψ2 because of the presence of its loci. Thus, the workspace bound by these singularity loci is termed the theoretical workspace.
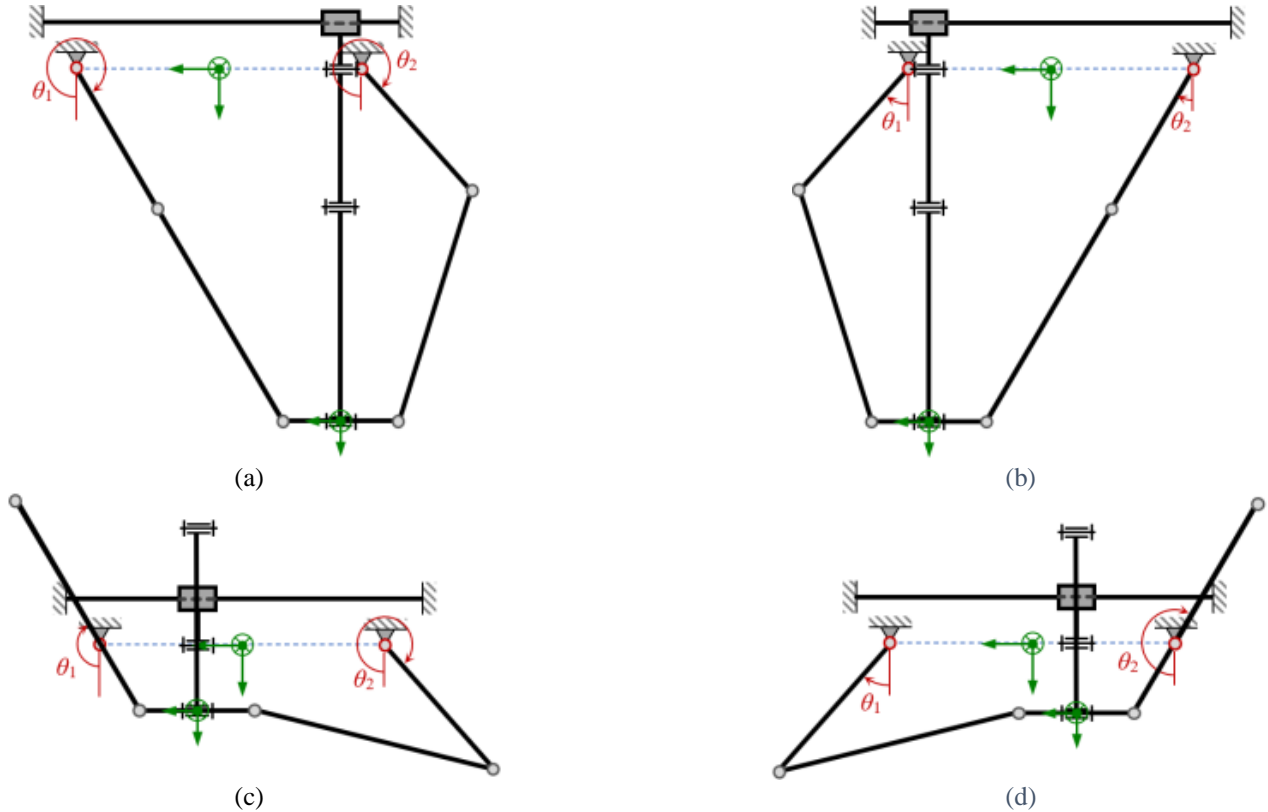

Fig. 6. An example of a singularity configuration of the first kind is when the distal and proximal links are perfectly extended at (a) the first and (b) the second active limbs and when both links are perfectly folded at (c) the first and (d) the second active limbs.

The second kind of singularity or direct kinematic singularity occurs when the matrix $\mathbf{J}_x$ is ill-conditioned. It is stated mathematically by $|\mathbf{J}_x| = 0$ [22], or

$$\begin{aligned} &(x_1 - a\sin\theta_1)(z - a\cos\theta_2) \\ &- (x_2 - a\,\sin\theta_2)(z - a\cos\theta_1) = 0. \end{aligned} \qquad (16)$$

Eq. 16 implies that the proximal links of both limbs are parallel to each other or in line with the platform, see Fig. 7. This second kind of singularity occurs inside the theoretical workspace. It splits the theoretical workspace into several parts because of its singularity loci. Thus, the largest nonsingular part is taken as the usable workspace.
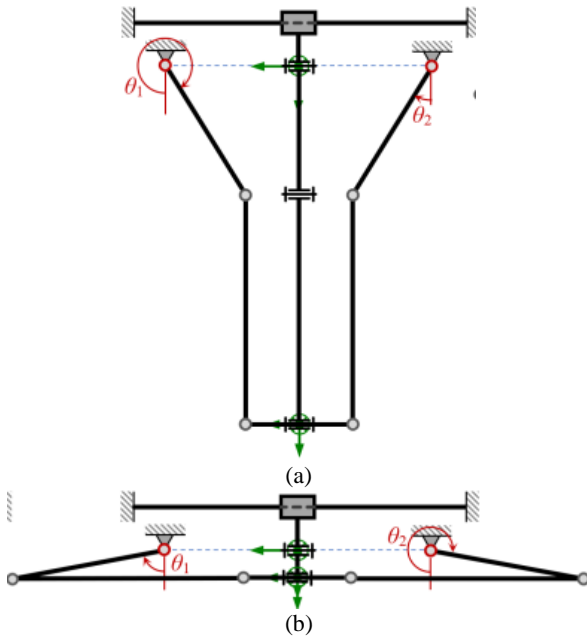
Fig. 7. An example of a singularity configuration of the second kind is when the proximal links in the active limbs are (a) parallel and (b) colinear to the platform.
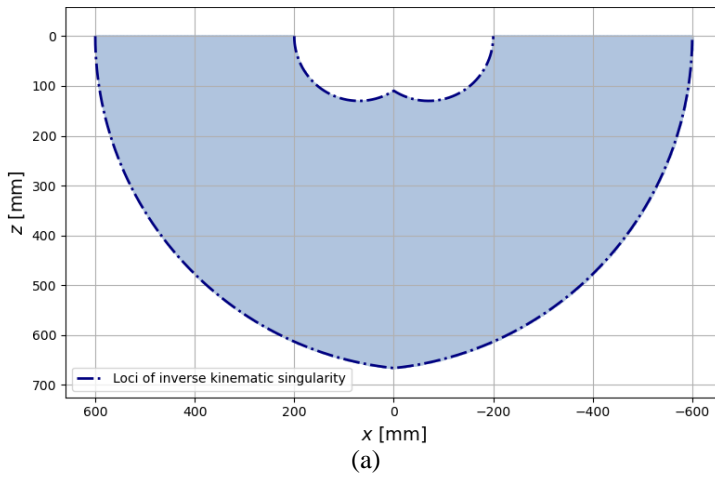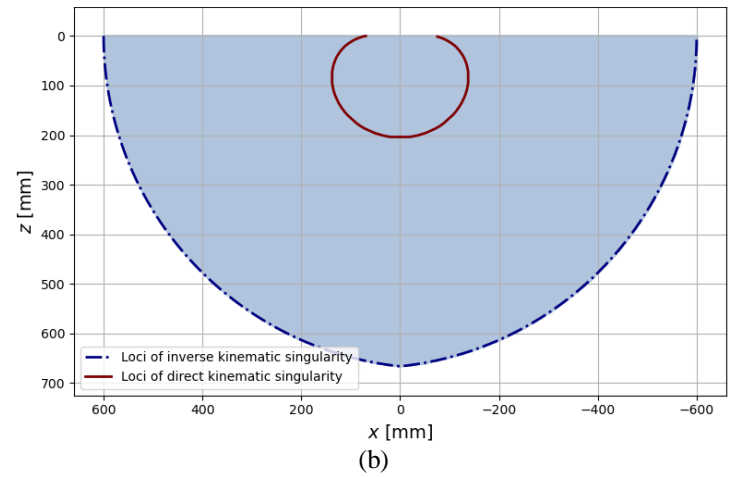
Moreover, the third kind of singularity, or combined kinematic singularity, occurs when both matrices $\mathbf{J}_q$ and $\mathbf{J}_x$ are rank deficient at the same time [22]. This leads to the intersection between loci of the inverse and direct kinematic singularities. This kind of singularity exists for special kinematic parameters. For instance, $\Psi2$ with $r_B = r_P$ produces loci of inverse kinematic singularity that coincide with loci of direct kinematic singularity.

The singularities of $\Psi2$ can be evaluated numerically using the kinematic parameters given in Table 1. The boundary for its workspace, as the loci of inverse kinematic singularity, is determined by the condition for the first kind of singularity, Eq. 15, as shown in Fig. 8. Applying the condition given by Eq. 16 results in the loci of direct kinematic singularity.

$\Psi2$ of Case #1 shows that only the loci of the inverse kinematic singularity bound its theoretical workspace. This means that the usable workspace is the theoretical workspace itself. Moreover, the $\Psi2$ of Case #2 presents loci of direct kinematic singularity inside its theoretical workspace. Hence, a workspace with no singularity inside can be extracted by removing an area enveloped by the loci of direct kinematic singularity; this workspace is referred to as the usable workspace [22]. Thus, the intersection of these two loci is the loci for combined kinematic singularity, which is not present for both cases.

Fig. 8. The singularity loci and workspace of $\Psi2$ for (a) Case #1 and (b) Case #2.
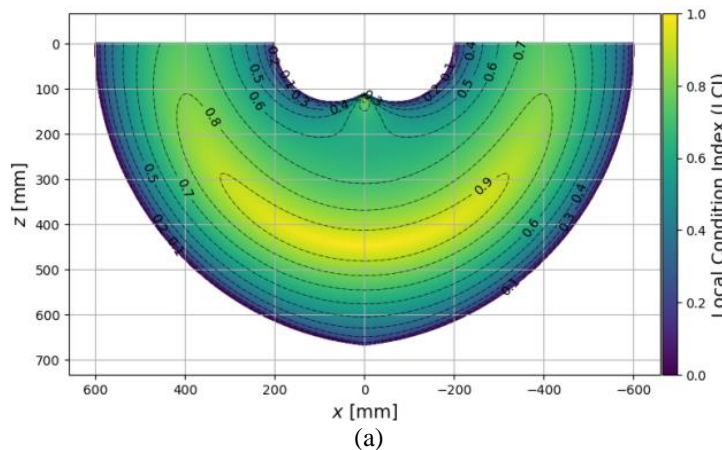
3.5 Workspace Identification

The useful workspace required for pick-and-place operation is identified by relying on the conditioning index. The conditioning index can be computed by first calculating its condition number using the Jacobian matrix, Eq. 14, which is defined as Eq. 17 [22]:

$$\kappa = \|\mathbf{J}^{-1}\| \, \|\mathbf{J}\|; \quad 1 \leqslant \kappa < \infty, \tag{17}$$

where $\|\ldots\|$ denotes the Euclidean norm of a matrix.

The performance index called the Local Condition Index (LCI), is calculated as an inverse of this condition number [22]

$$\text{LCI} = 1/\kappa; \quad 0 \leqslant \text{LCI} \leqslant 1. \tag{18}$$

Using the information given in Table 1, the LCI distribution of $\Psi2$ over the usable workspace can be plotted for each respective case as shown in Fig. 9. Each visualization is shown in a contour plot where an interval of 0.1 is applied to indicate the value of LCI from 0 to 1, in addition to the use of the color map.
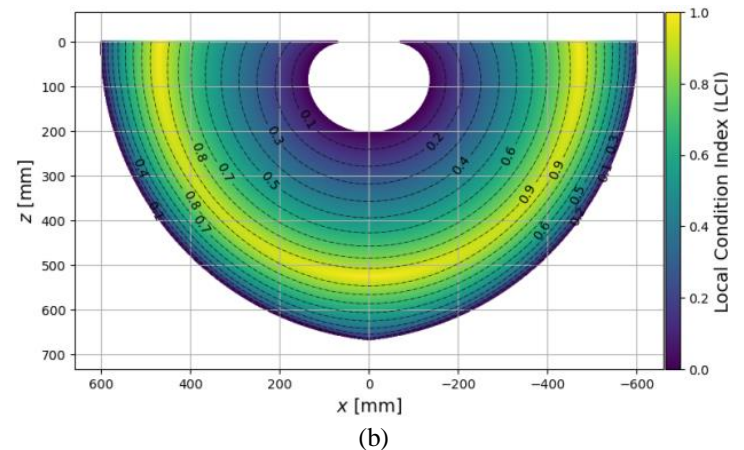

Fig. 9. The distribution of LCI values across the usable workspace for $\Psi2$ with kinematic parameters in (a) Case #1 and (b) Case #2.

A usable workspace with an LCI greater than 0.5 can be regarded as a Good Conditioning Workspace (GCW) [22]. These GCWs occupy approximately 78.40% and 58.74% of the usable workspace area for Case #1 and #2, respectively. In terms of this ratio, the $\Psi 2$ with kinematic parameters in Case #1 has a larger GCW than that in Case #2. Hence, it can be directly correlated to the area required by the useful workspace for pick-and-place operation. The largest rectangular area inside this GCW can be identified for both cases using a rectangular shape, see Fig. 10. This rectangular shape is symmetric about the Z-axis.
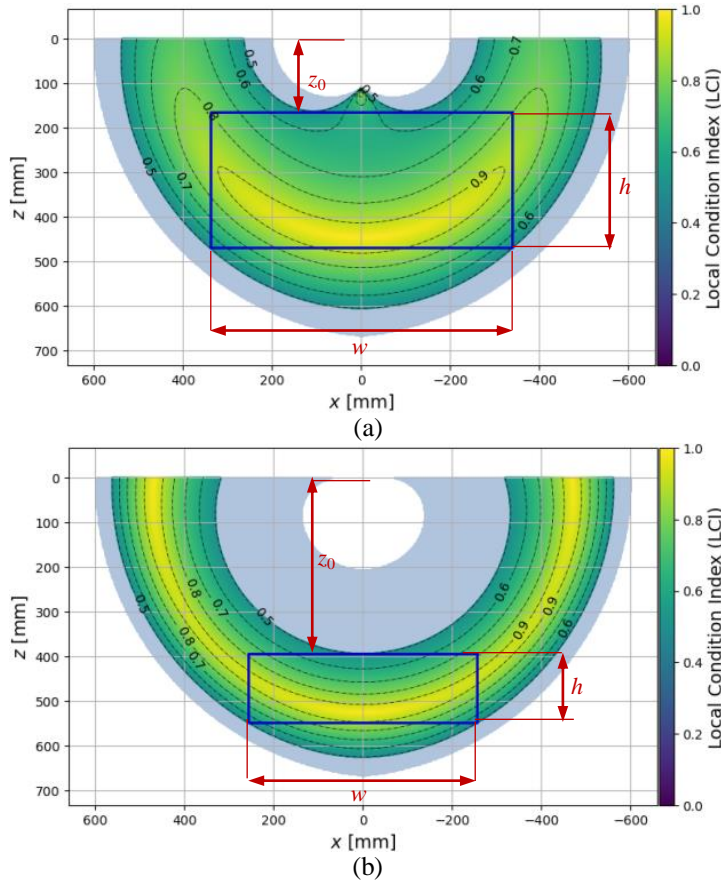

(a)

(b)

Fig. 10. The identified operational workspace of $\Psi 2$ for (a) Case #1 and (b) Case #2.

The largest rectangular area within the GCW is referred to as the identified operational workspace for the pick-and-place operation or simply as the operational workspace. The identified operational workspace is characterized by three parameters: the vertical position of the upper edge from the center of the fixed reference frame (z_0), the width (w), and the height (h) of the rectangle. Therefore, these parameters and their corresponding areas are presented in Table 3.

Table 3. The identified operational workspace for both cases of $\Psi 2$ in a rectangular shape.

Workspace	Case #1	Case #2
z_0 [mm]	163.48	393.96
h [mm]	305.52	154.10
w [mm]	677.84	512.08
Area [mm^2]	207 093.68	78 911.53

Furthermore, the percentages of the operational workspace to the GCW for Cases #1 and #2 are 46.18% and 23.68%, respectively. Additionally, it is customary to compare the operational workspace to the usable workspace. The operational workspace of $\Psi 2$ in Case #1 accounts for 36.21% of its usable workspace, while that in Case #2 is 13.91%. Only a small portion of the (usable or good conditioning) workspace is suitable for pick-and-place operation. Thus, $\Psi 2$ with equal length of proximal

and distal links gives a small operational workspace compared to $\Psi 2$ with unequal length, i.e. the distal link is shorter than the proximal one. Therefore, this study is in agreement with any optimal design of PMs such as IRSBot-2 [17], Par2 [15], DexTAR [11], or 5R PPM [10], [28], [29].

Information about the width of the identified useful workspace (w) can be used to determine the appropriate stroke of prismatic or cylindrical joints in the passive limbs. In practical applications, the use of cylindrical joints may be preferable to reduce joint type complexity [18]. However, the use of a prismatic joint may be a viable option from a static point of view. In addition, the prismatic joints on each passive limb can be connected during the operation. This connection can maintain the synchronization of both passive limbs during translational motion along the X-axis, as shown in Fig. 11. Further investigation can be performed in the future to clarify this argument.
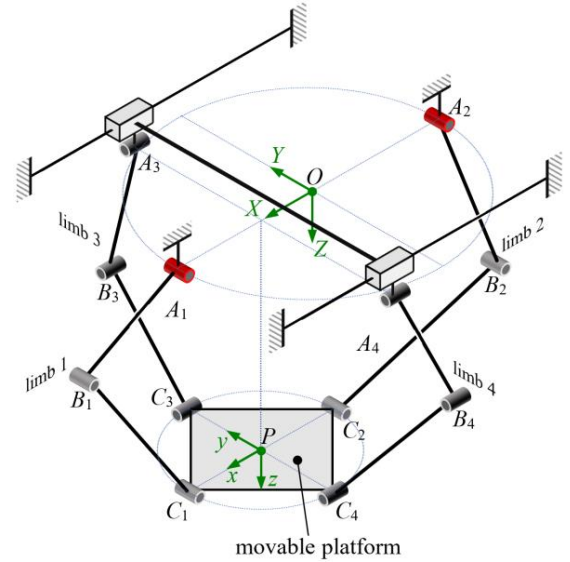

Fig. 11. $\Psi 2$ with a rigid connection between the prismatic joints of each passive limb.

Overall, $\Psi 2$ is an excellent candidate for high-speed pick-and-place operation in terms of kinematic, singularity, and workspace analysis.

4 Conclusion

This research proposed a new spatial PM with pure translational motion in a plane, named $\Psi 2$, for pick-and-place operation. The architecture of $\Psi 2$ is described in detail, including its kinematic parameters. Kinematic analysis of $\Psi 2$ shows that its inverse and direct kinematic problems have closed-form solutions. These closed-form solutions are evaluated by the predetermined values of the kinematic parameters of $\Psi 2$, which are verified by the solutions throughout the interval analysis. Moreover, the usable workspace of $\Psi 2$ can be determined based on singularity analysis. A portion of the usable workspace with a good conditioning index has been successfully identified as the operational workspace for pick-and-place operation. A dimensional synthesis will be performed in future research to determine an optimized dimension for each kinematic parameter considering the prescribed operational workspace within good conditioning and good transmission workspaces. Afterward, dynamic analysis and designing of the control system can be conducted by using the optimized dimensions. As a result, the peak acceleration of $\Psi 2$ can be determined to obtain how quickly it can be operated for pick-and-place operation.

Acknowledgment

References

[1] Z. Wang, S. Hirai, and S. Kawamura, "Challenges and Opportunities in Robotic Food Handling: A Review," *Front. Robot. AI*, vol. 8, no. January, pp. 1–12, 2022, doi: 10.3389/frobt.2021.789107.

[2] H. Makino, "Development of the SCARA," *J. Robot. Mechatronics*, vol. 26, no. 1, pp. 5–8, 2014, doi: 10.20965/jrm.2014.p0005.

[3] Q. Meng, X. J. Liu, and F. Xie, "Design and development of a Schönflies-motion parallel robot with articulated platforms and closed-loop passive limbs," *Robot. Comput. Integr. Manuf.*, vol. 77, no. 102352, 2022, doi: 10.1016/j.rcim.2022.102352.

[4] Z. Zhang *et al.*, "State-of-the-art on theories and applications of cable-driven parallel robots," *Front. Mech. Eng.*, vol. 17, no. 3, 2022, doi: 10.1007/s11465-022-0693-3.

[5] V. Nabat, M. De La O Rodriguez, O. Company, S. Krut, and F. Pierrot, "Par4: Very high speed parallel robot for pick-and-place," in *IEEE/RSJ International Conference on Intelligent Robots and Systems, IROS*, 2005, pp. 553–558, doi: 10.1109/IROS.2005.1545143.

[6] S. Briot and I. A. Bonev, "Pantopteron-4: A new 3T1R decoupled parallel manipulator for pick-and-place applications," *Mech. Mach. Theory*, vol. 45, no. 5, pp. 707–721, 2010, doi: 10.1016/j.mechmachtheory.2009.07.007.

[7] F. Xie and X. J. Liu, "Design and development of a high-speed and high-rotation robot with four identical arms and a single platform," *J. Mech. Robot.*, vol. 7, no. 4, pp. 041015 1–12, 2015, doi: 10.1115/1.4029440.

[8] Q. Meng, F. Xie, S. Zhang, and X. Liu, "Type Synthesis and Dimensional Optimization of a High-speed and High-acceleration Parallel Robot," *J. Mech. Eng.*, vol. 58, no. 13, pp. 36–49, 2022, doi: 10.3901/JME.2022.13.036.

[9] T. Huang, Z. Li, M. Li, D. G. Chetwynd, and C. M. Gosselin, "Conceptual design and dimensional synthesis of a novel 2-DOF translational parallel robot for pick-and-place operations," *J. Mech. Des. Trans. ASME*, vol. 126, no. 3, pp. 449–455, 2004, doi: 10.1115/1.1711822.

[10] X. J. Liu, J. Wang, and G. Pritschow, "Performance atlases and optimum design of planar 5R symmetrical parallel mechanisms," *Mech. Mach. Theory*, vol. 41, no. 2, pp. 119–144, 2006, doi: 10.1016/j.mechmachtheory.2005.05.003.

[11] L. Campos, F. Bourbonnais, I. A. Bonev, and P. Bigras, "Development of a five-bar parallel robot with large workspace," in *Proceedings of the ASME Design Engineering Technical Conference*, 2010, vol. 28962, pp. 917–922, doi: 10.1115/DETC2010-28962.

[12] O. Stepanenko and I. A. Bonev, "Novel 4-DOF SCARA Parallel Robot With Cylindrical Workspace," in *Proceedings of the ASME Design Engineering Technical Conference and Computers and Information in Engineering Conference*, 2018, vol. 86113, pp. 1–7, doi: 10.1115/DETC201886113.

[13] Q. Meng, F. Xie, and X. J. Liu, "V2: A novel two degree-of-freedom parallel manipulator designed for pick-and-place operations," in *2017 IEEE International Conference on Robotics and Biomimetics (ROBIO)*, 2017, vol. 2018-Janua, no. January 2019, pp. 1320–1327, doi: 10.1109/ROBIO.2017.8324600.

[14] S. E. E. Profile, S. E. E. Profile, and S. E. E. Profile, "Par2: a Spatial Mechanism for Fast Planar, 2-dof, Pick-and-Place Applications," 2008.

[15] O. Company, F. Pierrot, S. Krut, C. Baradat, and V. Nabat, "Par2: A spatial mechanism for fast planar two-degree-of-freedom pick-and-place applications," *Meccanica*, vol. 46, no. 1, pp. 239–248, 2011, doi: 10.1007/s11012-010-9413-x.

[16] C. Germain, S. Briot, V. Glazunov, S. Caro, and P. Wenger, "IRSBOT-2: A novel two-DOF parallel robot for high-speed operations," in *Proceedings of the ASME 2011 International Design Engineering Technical Conferences & Computers and Information in Engineering Conference*, 2011, pp. 1–11, doi: 10.1115/DETC2011-47564.

[17] S. Briot, S. Caro, and C. Germain, "Design procedure for a fast and accurate parallel manipulator," *J. Mech. Robot.*, vol. 9, no. 6, pp. 1–11, 2017, doi: 10.1115/1.4038009.

[18] L. Nurahmi, "Conceptual Design and Analysis of 2 Degrees of Freedom Translational Parallel Manipulators," Ecole Centrale de Nantes, 2012.

[19] H. L. Vieira, A. T. Beck, and M. M. da Silva, "Combined interval analysis - Monte Carlo simulation approach for the analysis of uncertainties in parallel manipulators," *Meccanica*, vol. 56, pp. 1867–1881, 2021, doi: 10.1007/s11012-021-01359-7.

[20] X. Jin, X. Jiang, and Q. Li, "Interval-analysis-based determination of the trajectory-reachable workspace of planar cable-suspended parallel robots," *Mech. Mach. Theory*, vol. 177, 2022, doi: 10.1016/j.mechmachtheory.2022.105060.

[21] R. E. Moore, R. B. Kearfott, and M. J. Cloud, *Introduction to Interval Analysis*. Society for Industrial and Applied Mathematics, 2009.

[22] X. J. Liu and J. Wang, *Parallel Kinematics-Type, Kinematics, and Optimal Design*. Berlin: Springer-Verlag, 2014.

[23] C. R. Harris *et al.*, "Array programming with NumPy," *Nature*, vol. 585, no. 7825, pp. 357–362, 2020, doi: 10.1038/s41586-020-2649-2.

[24] L. Benet and D. P. Sanders, "JuliaIntervals - Guaranteed computations." 2022.

[25] Y. Li, L. Wang, J. Liu, and Z. Huang, "Applicability and generality of the modified Grübler-Kutzbach criterion," *Chinese J. Mech. Eng. (English Ed.*, vol. 26, no. 2, pp. 257–263, 2013, doi: 10.3901/CJME.2013.02.257.

[26] S. Caro, W. A. Khan, D. Pasini, and J. Angeles, "The Rule-based Conceptual Design of the Architecture of Serial Schonflies-motion Generators," *Mech. Mach. Theory*, vol. 45, no. 2, p. 2, 2010, doi: 10.1016/j.mechmachtheory.2009.09.002.

[27] Z. Xie and Q. Lin, "Reinforcement Learning-Based Adaptive Position Control Scheme for Uncertain Robotic Manipulators with Constrained Angular Position and Angular Velocity," *Appl. Sci.*, vol. 13, no. 3, 2023, doi: 10.3390/app13031275.

[28] L. Wang, Z. Zhang, Z. Shao, and X. Tang, "Analysis and optimization of a novel planar 5R parallel mechanism with variable actuation modes," *Robot. Comput. Integr. Manuf.*, vol. 56, pp. 178–190, 2019, doi: 10.1016/j.rcim.2018.09.010.

[29] Adriyan, "Sintesis Dimensi Manipulator Paralel Bidang Dua Derajat Kebebasan Dengan Rantai Kinematik Paralelogram Simetris," *Met. J. Sist. Mek. dan Termal*, vol. 5, no. 2, pp. 72–85, 2021.